Ignition and Combustion of Fuel Pockets Moving in an Oxidizing Atmosphere

JOEL DAOU

Dpto. Motopropulsion y Termofluidodinamica, Universidad Politecnica De Madrid, E.T.S.I Aeronauticos, 28040 Madrid, Spain. E-mail: daou@tupi.dmt.upm.es

Ignition and combustion of an initially spherical pocket of fuel in motion relative to a hot oxidizing atmosphere is studied. The model considers finite rate chemistry represented by an irreversible one-step reaction. Attention is focused on the development of the ignition process, which, in the end, typically leads to the establishment of a diffusion flame. For moderate values of a suitably defined Damköhler number, three stages are identified in the burning process. Stage I corresponds to an induction period during which a mixing layer is formed around the fuel kernel. This stage ends up with a thermal runaway close to the back of the kernel. Stage II involves the propagation of a chemical front in the mixing layer: initiated at the point where the thermal runaway occurs, a first flame travels around the fuel kernel towards the nose, triggering during its travel a premixed radial inwardly propagating flame. The second stage ends when ignition reaches the nose. Stage III corresponds to an established diffusive burning, which is most active at the front surface.

As the Damköhler number, Da, is increased, stage I and II shrink leading to a practically spherical ignition. In this limit of large Da, the ignition time becomes independent of the Reynolds number. Conversely, for sufficiently low Da, stage III (i.e., diffusive burning) is absent. In this case, the fuel is practically consumed by reaction at the back of the kernel, after premixing at the front mixing layer with the oxidizer. The flame responsible for the burning occupies a quasi-steady stable position close to the maximum cross section position.

Furthermore, the results provide a good appreciation of the dynamics of the combustion process. For example, it is found for moderate Da that a significant acceleration-deceleration of the fuel pocket takes place during ignition due to the pressure increase caused by gas expansion. Finally, with the aid of an order-of-magnitude analysis, a synthesis of most of the physical results described above is achieved by delimiting different domains in the Da-Re plane.

NOMENCLATURE

a_0	initial radius of the fuel kernel
c_p	specific heat of mixture
Da	Damköhler number defined in Eq. (9)
E	activation energy
F	fuel (or initial component of the dense kernel)
Le_1	fuel Lewis number
Le_2	oxidizer Lewis number
Ox	oxidizer
P	combustion products
p	pressure
Pr	Prandtl number
Q	heat release per unit mass of fuel
q	nondimensional heat release, see Eq. (8)
Re	Reynolds number $\equiv \rho_\infty a_0 U_0/\mu$
s	stoichiometric coefficient, $s \equiv \nu Y_{1,0}/Y_{2,\infty}$
T	temperature (dimensional)
T_∞	temperature in the far field
t	time
t_L	planar premixed flame time, see Eq. (18)
U_0	initial velocity of the fuel kernel
$\boldsymbol{v}$	velocity vector (in a frame at rest with the fluid at infinity)
x	coordinate in the axial direction
Y_1	fuel mass fraction
Y_2	oxidizer mass fraction (normalized by its value at infinity)
Ze	Zeldovich number
β	nondimensional activation energy, see Eq. (11)
ϵ^{-1}	density ratio $\equiv \rho_0/\rho_\infty$
μ	dynamic viscosity
ν	stoichiometric coefficient, see (1)
ρ	density (nondimensionalized by its value at infinity)
ρ_0	initial density of the fuel kernel
ρ_∞	density in the far field
σ	defined in Eq. (20)
θ	temperature (nondimensionalized by its value at infinity)
ω	(fuel-) consumption rate

*Corresponding author:

COMBUSTION AND FLAME 115:383–394 (1998)

Published by Elsevier Science Inc.

0010-2180/98/$19.00
PII 0010-2180(98)00005-4

Ω nondimensional fuel consumption rate
Ω_q nondimensional heat release rate $\equiv q\Omega$.

Subscripts

ad adiabatic
max indicates a spatial maximum
0 indicates initial values of fuel kernel
1 relative to the fuel
2 relative to the oxidizer
∞ indicates the values in the far field

Superscripts

0 indicates values relative to a planar configuration

INTRODUCTION

This paper is concerned with the ignition and combustion of an initially spherical kernel of fuel in motion relative to a hot oxidizer. The study is essentially devoted to the initiation and dynamics of burning of fuel drops in supercritical conditions, where a liquid droplet is modeled as a puff of a dense gas under the assumption that its interface has been heated to above its critical temperature. Because of its relevance to high-pressure combustion devices, the supercritical regime and the conditions under which it is attained has been the subject of a number of analytical, experimental, and numerical studies [1–8]. It is relevant here to note that, although the bulk of the literature has considered the vaporization/combustion of a droplet in a quiescent environment, studies under forced convection are also available [9–12]. Nevertheless, almost all the studies in the convective case have neglected droplet deformation, that is, considered effectively the limit of small Weber numbers (i.e., strong surface tension). Under this restriction, analytical studies [9, 10] have been based on a boundary-layer analysis at the front surface of the droplet, which typically leads to gasification/combustion times inversely proportional to the square root of a suitably defined diffusion coefficient. Account for non-small, but finite values, of the Weber number has been taken in the numerical study by Deng et al. [13] and has been found to result in an increase in the overall vaporization rate due to deformation.

Recently, a few studies have addressed the supercritical case under forced convection, a case that can be viewed as corresponding to the limit of infinite Weber number. Lee et al. investigated how a puff of gas mixes with the ambient gas in the frame of a constant density assumption [14]; they described the enhancement of mixing induced by the flow. More recently, Daou and Haldenwang have examined the similar problem of the heat-mixing accompanying the injection of a cold puff of gas into a hot environment [15]; they exhibited in particular the asymptotic behaviour of mixing time for high Reynolds numbers. Daou and Rogg extended the preceding investigation to combustion situations in the frame of a flame sheet model and examined in particular the effect of heat release on the combustion rate [16]. The last two studies have put forward a square-root dependence of the mixing (respectively, burnout) time on density ratio,[1] along with its independence of diffusion coefficients as soon as the Reynolds number[2] exceeds a few hundreds.

Both the non-reactive and reactive cases just described have been also considered independently by Umemura and Jia under closely related conditions [17]. It is instructive to examine the similarities and the complementary aspects of the findings in [15, 17].

The main object of the present study is to investigate features of convective burning of supercritical droplets related to finite rate effects associated with the chemistry. In particular we shall describe the development of ignition and determine the conditions of occurrence of different burning regimes. Because fluid mechanical aspects of the problem (such as deformation, drag, and breakup) have been addressed elsewhere [5, 15, 16], we shall give no detailed discussion of these aspects and also restrict ourselves in the numerical simulations to moderate values of the Reynolds number Re (say, Re of the order of a few tens). The paper is organized as follows. First the physical model

[1] Defined as the density of the initial kernel divided by the density of the surrounding gas.
[2] Based on initial radius and velocity of the pocket and on background properties.

is presented. This model includes a simplified version of transport properties, which are assumed to be constant except for density, which is taken to follow the perfect gas law. Also the chemistry is represented by a single irreversible Arrhenius reaction. Although a more sophisticated modeling of thermo-physical properties and chemistry is available and can be easily incorporated, we deliberately adopt the above simplifications in order to facilitate understanding of the results.

Presentation of the results begins with an illustrative case, where three stages leading to an established diffusion flame are identified. Then the influence of the Damköhler number, Da, is addressed, followed by examination of the behaviour of the ignition time. Finally an order-of-magnitude analysis is provided allowing classification and synthesis of the main results in a Da-Re diagramme.

MODEL

The problem to be studied herein is the initiation and combustion process around an initially spherical kernel of fuel, which is suddenly set into motion in a hot oxidizing atmosphere. For sake of simplicity, the following assumptions are adopted. Axisymmetric flow at low Mach numbers is considered. The thermal conductivity, the heat capacity c_p, the molecular weight and the dynamic viscosity μ of the gas mixture as well as the products of the density with the individual species diffusion coefficients are taken as constant. The combustion is represented by a single irreversible one-step reaction of the form

$$\mathrm{F} + \nu\mathrm{Ox} \rightarrow \mathrm{P} + Q, \tag{1}$$

where F denotes the fuel, Ox the oxidizer, and P the products. The quantity ν denotes the mass of oxidizer consumed and Q the heat released, both per unit mass of fuel. The combustion rate, ω defined as the mass of fuel consumed by unit volume and unit time is assumed to follow an Arrhenius law of the form:

$$\omega = \rho B Y_1 Y_2 e^{-E/RT}, \tag{2}$$

where ρ, B, Y_1, Y_2, and E/R represent respectively density, the (constant) pre-exponential factor, mass fraction of fuel, mass fraction of oxidizer, and the activation temperature.

Under the above assumptions, the governing equations can be written in non-dimensional form as

$$\frac{\partial \rho}{\partial t} + \nabla \cdot (\rho \boldsymbol{v}) = 0, \tag{3}$$

$$\rho \frac{\partial \boldsymbol{v}}{\partial t} + \rho \boldsymbol{v} \cdot \nabla \boldsymbol{v} = -\nabla p + \mathrm{Re}^{-1} \Delta \boldsymbol{v}, \tag{4}$$

$$\rho \frac{\partial Y_1}{\partial t} + \rho \boldsymbol{v} \cdot \nabla Y_1 = (\mathrm{Re\ Pr\ Le}_1)^{-1} \Delta Y_1 - \mathrm{Da}\ \Omega, \tag{5}$$

$$\rho \frac{\partial Y_2}{\partial t} + \rho \boldsymbol{v} \cdot \nabla Y_2 = (\mathrm{Re\ Pr\ Le}_2)^{-1} \Delta Y_2 - s\ \mathrm{Da}\ \Omega, \tag{6}$$

$$\rho \frac{\partial \theta}{\partial t} + \rho \boldsymbol{v} \cdot \nabla \theta = (\mathrm{Re\ Pr})^{-1} \Delta \theta + q\ \mathrm{Da}\ \Omega, \tag{7}$$

Here t, θ, ρ, $\boldsymbol{v}$, and p are non-dimensional but otherwise have their usual meaning of time, temperature, density, velocity, and (modified) pressure, respectively. For non-dimensionalisation we have adopted as basic units the following quantities: initial kernel radius a_0, initial kernel velocity U_0, and density and temperature in the far field. The mass fractions of fuel, Y_1, has been normalized by its initial value at the origin $Y_{1,0}$, which will be taken equal to one; the mass fraction of the oxidizer, Y_2, has been normalized by its (initial) value at infinity, $Y_{2,\infty}$. Re, Pr, Le_1, and Le_2 are the Reynolds number, Prandtl number, the fuel Lewis number, and the oxidizer Lewis number, respectively; s is the stoichiometric coefficient, $s \equiv \nu Y_{1,0}/Y_{2,\infty}$, and q the nondimensional heat release parameter defined by

$$q \equiv \frac{Q Y_{1,0}}{c_p T_\infty}. \tag{8}$$

Da is the Damköhler number equal to the initial convective time divided by a characteristic chemical time in the far field, namely,

$$\mathrm{Da} \equiv \frac{a_0/U_0}{(B Y_{2,\infty} e^{-E/RT_\infty})^{-1}}. \tag{9}$$

As a consequence of this choice the non-dimensional reaction rate Ω as appearing in the governing equations is given by

$$\Omega = \rho Y_1 Y_2 e^{-\beta(1/\theta - 1)}, \tag{10}$$

where

$$\beta \equiv \frac{E}{RT_\infty} \tag{11}$$

is the non-dimensional activation energy. Finally we adopt the ideal gas equation of state; hence

$$\rho\theta = 1. \tag{12}$$

The initial conditions at $t = 0$ correspond to a spherical kernel of fuel with non-dimensional radius of unity, which is placed around the origin. Inside the kernel, the initial values $Y_1 = 1$, $Y_2 = 0$, $\theta = \epsilon$, and $\boldsymbol{v} = \boldsymbol{e}_x$ are adopted. Here ϵ denotes the ratio $\epsilon \equiv T_0/T_\infty$, where T_0 and T_∞ are the initial temperature of the fuel and the surrounding respectively; $\boldsymbol{e}_x$ is the unit vector in the axial direction. Outside the kernel, we take $Y_1 = 0$, $Y_2 = 1$, $\theta = 1$, and $\boldsymbol{v} = \boldsymbol{0}$. The boundary conditions correspond to a stagnant hot atmosphere at infinity, which contains oxidizer but no fuel. Thus infinitely far away from the kernel we have $Y_1 = 0$, $Y_2 = 1$, $\theta = 1$, and $\boldsymbol{v} = \boldsymbol{0}$. In the present study the computations were performed for different values of Da and Re, and the values adopted for the other governing parameters were $\beta = 10$, $s = 1$, $q = 5$, $\epsilon = 0.1$, and $\mathrm{Le}_1 = \mathrm{Le}_2 = 1$.

Numerical Considerations

Equations (3)–(7), in cylindrical coordinates, are discretized using a finite volume method and solved with a multigrid method [18]. The extent of the computational domain in both the axial and radial direction is taken to be 50 times the initial radius a_0. After each time step, the solution of the governing equations is remapped to the domain such that the dense kernel remains located approximately at the origin of the coordinate system. The grid is a non-uniform rectangular grid with typically 400×200 grid points.

RESULTS

In the present section, the results are presented as follows. First a typical case is considered where the dynamics and the burning of the moving fuel kernel are described. In particular, three stages are identified in the combustion process. Second, for a fixed value of the Reynolds number, the influence of Damköhler number is investigated. Third, for a fixed value of Da, the influence of Reynolds number on the ignition time is considered. Fourth an order of magnitude analysis is presented, allowing to interpret and classify the results in the Da-Re plane.

Presentation of a First, Illustrative Case

In this section, we describe the evolution of the fuel kernel, starting at time $t = 0$ at which it is put abruptly into motion until its complete consumption through chemical reaction has occurred. The parameters for this first, illustrative case take the values $\mathrm{Re} = 10$, $\mathrm{Da} = 1$, and $\epsilon = 0.1$. Shown in Fig. 1a, b is a temporal sequence of pictures illustrating the ignition and combustion of a fuel kernel. The top picture in Fig. 1a pertains to $t = 0.96$, a time shortly after the kernel has been put into motion. The bottom picture in Fig. 1b pertains to $t = 11.04$, a time close to the end of the kernels lifetime. Colours describe the temperature field, and arrows represent the velocity field relative to a frame moving with an average kernel velocity U, which is defined as

$$U = \frac{\int_D \rho v_x \, \mathrm{d}\, D}{\int_D \rho \, \mathrm{d}\, D} \tag{13}$$

with the domain D being taken as the fuel containing region.[3]

In each picture of Fig. 1a, b, two iso-lines of fuel mass fraction have been included, viz., the dashed line corresponding to $Y_1 = 0.1$ and the full line corresponding to $Y_1 = 0.9$. From the sequence of pictures we note that, after an induction time of approximately $t = 1.4$ corresponding roughly to the second picture in Fig.

[3] The fuel containing region has been taken as that portion of the overall domain in which the mass fraction of fuel exceeds 0.01.

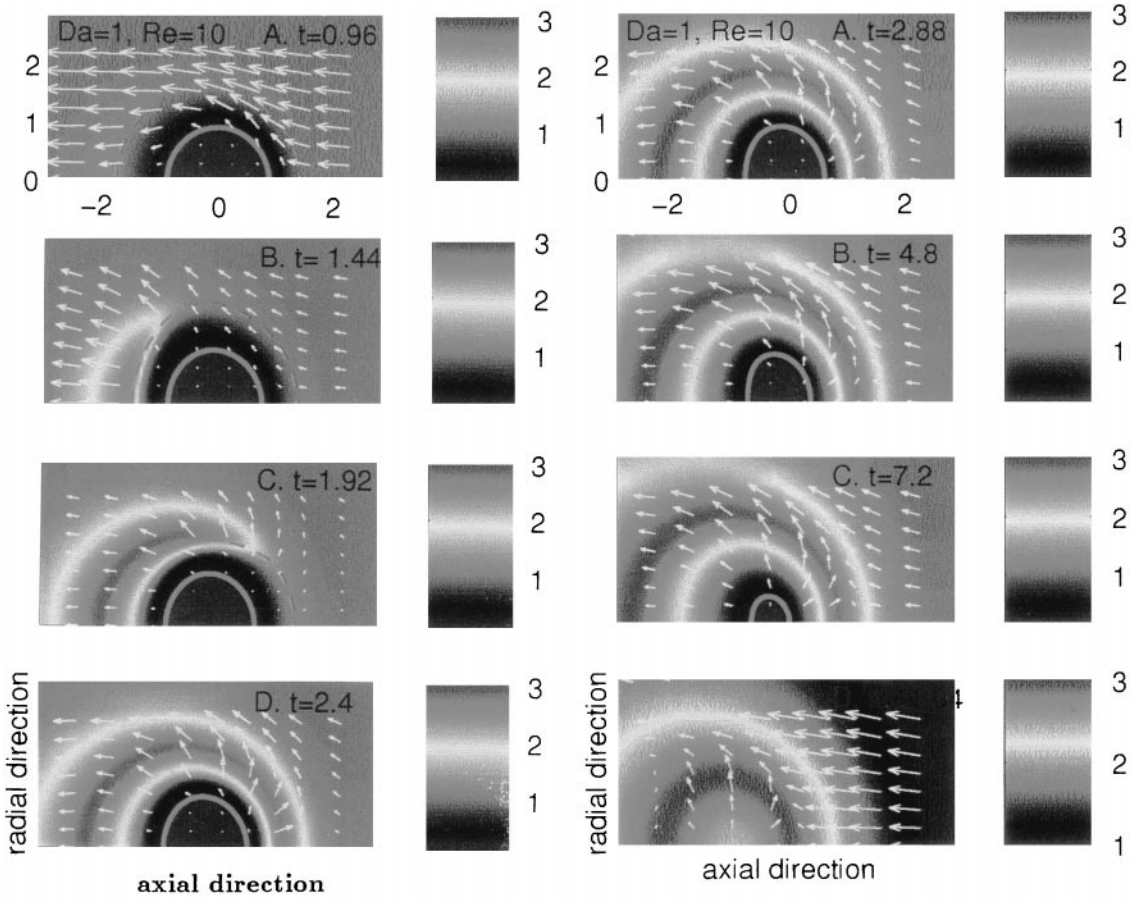

Fig. 1. A temporal sequence of pictures illustrating the ignition and combustion of a fuel kernel. The pictures pertain, respectively, to $t = 0.96$, 1.44, 1.92, 2.4, 2.88, 4.8, 7.2, and 11.04. The different gray shadings describe the temperature field and arrows represent the velocity field relative to a frame moving with the average kernel velocity. The parameters corresponding to this case are: Re = 10, Da = 1 and ($\epsilon = 0.1$, $\beta = 10$, $s = 1$, $q = 5$, $\mathrm{Le}_1 = \mathrm{Le}_2 = 1$). In each picture of a and b two iso-lines of fuel mass fraction have been included, viz., the dashed line corresponding to $Y_1 = 0.1$ and the full line corresponding to $Y_1 = 0.9$.

1a, thermal runaway takes place in the vicinity of the rear stagnation point of the kernel initiating there transient flame propagation around it. At some time corresponding to a time between that of the last two pictures of Fig. 1a, the propagating flame reaches the front stagnation point or nose. Thereafter, a diffusive burning phase is established which lasts until all fuel has been consumed.

Additional information on thermal runaway, flame propagation and diffusive burning can be obtained from Fig. 2a, b, which shows surface plots of the heat-release rate $\Omega_q \equiv q\Omega$ corresponding frame by frame to the individual pictures of Fig. 1. In addition to the information already gathered from Fig. 1, from Fig. 2 it is seen that during the phase of circumferential flame propagation, the flame propagates also in a direction pointing roughly radially inwards (as in the spherically symmetrical case) albeit at a substantially lower velocity than in the circumferential direction. Furthermore, it is seen from Fig. 2 that during the phase of diffusive burning chemical reaction is most active at the front surface where the diffusive fluxes of reactants are highest.[4]

A clear identification of the three stages (thermal runaway, flame propagation, and dif-

[4] Mainly due to negligible presence of combustion products that are convected downstream, as commonly observed in the studies of the convective combustion of drops.

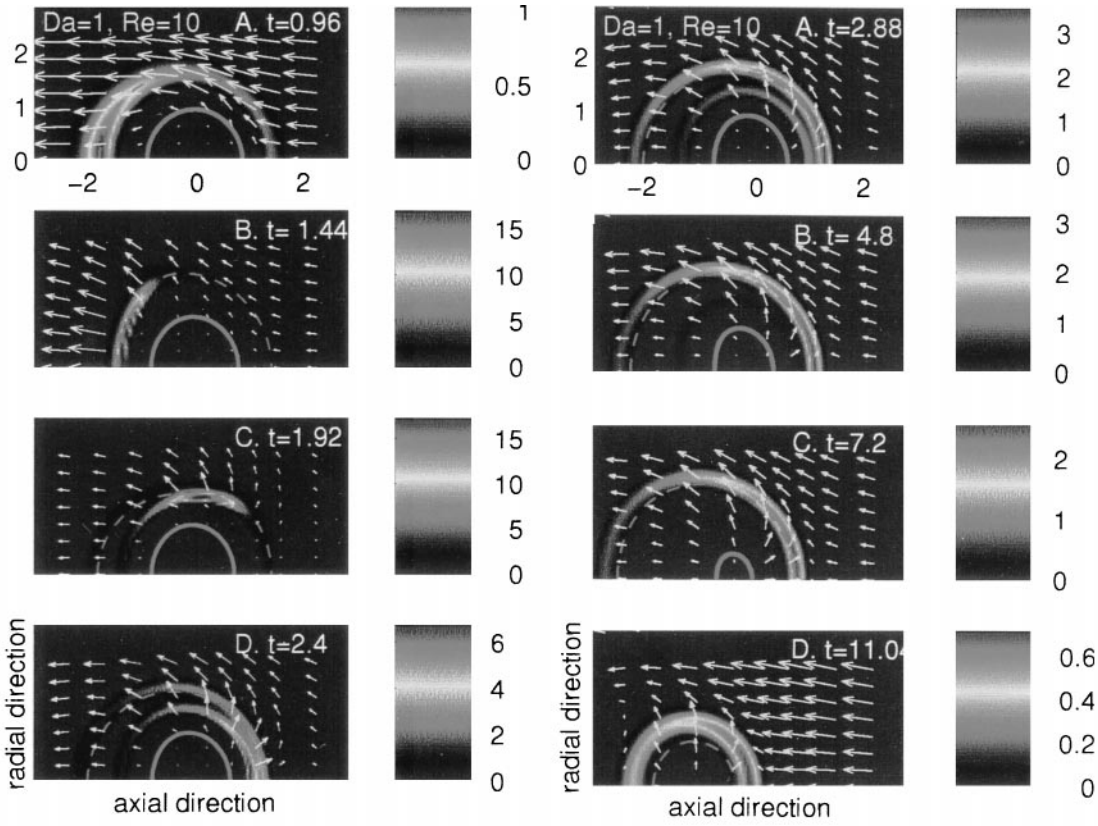

Fig. 2. Same as Fig. 1 with gray shadings, full and dashed lines now describing the heat-release rate Ω_q.

fusive burning) described above can be obtained by plotting the maximum rate of heat release Ω_q vs time as represented in Fig. 3. In this figure, these three stages are denoted by I, II, and III, respectively. Also plotted in this figure is the maximum temperature $\theta_{\max}$ vs time. It is seen that during most of the lifetime of the kernel $\theta_{\max}$ remains (slightly) lower than the adiabatic flame temperature given by

$$\theta_{\mathrm{ad}} \equiv \frac{T_{\mathrm{ad}}}{T_\infty} = \frac{1 + \epsilon + q}{1 + s} \tag{14}$$

and equal here to 3.05.

Finally, to complete the study of this case, shown in Fig. 4 is the variation versus time of the average velocity U of the fuel kernel (solid line) and of the total mass of fuel $m_{\mathrm{F}}(t)/m_{\mathrm{F}}(0)$ (dashed line). To identify in Fig. 3 the successive three stages, the maximum heat release rate discussed above is included as a dashed-dotted line. It is seen that, after the short initial stage of thermal runaway, fuel mass begins to decrease in appreciable amounts and fuel consumption is fastest during the stage of flame propagation. In particular, the almost linear decrease of the fuel mass during this stage is consistent with the plateau of Ω_q observed during that stage in Fig. 3. The kernel velocity U varies non-monotonically. After an initial decrease due to drag forces, the transition from stage I to stage II is accompanied by an increase of the kernel velocity, followed by a continuous decrease. This significant acceleration-deceleration of the kernel during ignition is associated with the corresponding decrease-increase of pressure drag acting on the kernel, accompanying gas expansion, due to combustion. (In other words, combustion starts at the back, resulting in an overpressure there, which leads to a propulsion of the kernel; the overpressure then moves with the premixed flame circumferentially around the kernel and tends to slow down the kernel as it approaches the nose.)

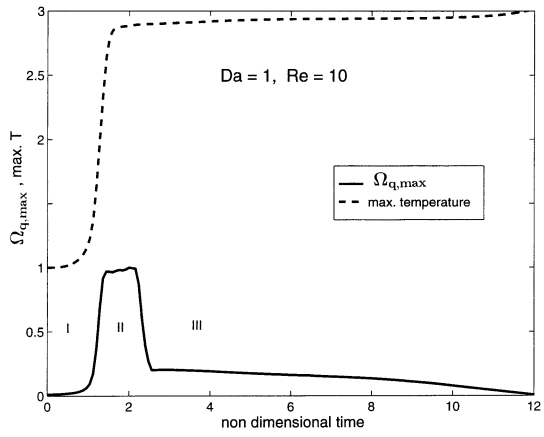

Fig. 3. Maximum rate of heat release $\Omega_{q,\max}$ (solid line) and maximum temperature $\theta_{\max}$ (dashed line) versus time. The solid line delimits three stages in the burning process (thermal runaway, flame propagation and diffusive burning) denoted by I, II, and III, respectively. Same parameters as in Fig. 1.

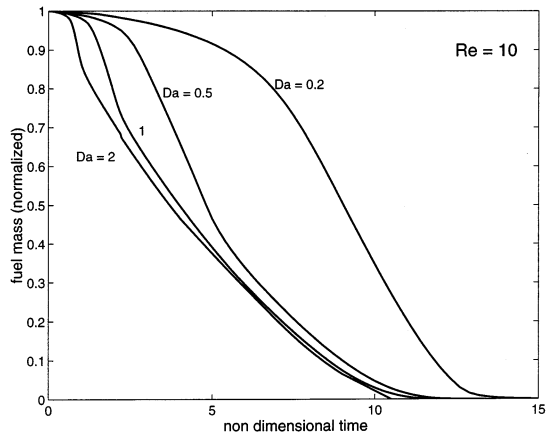

Fig. 5. Total mass of fuel versus time for Re = 10 and four values of Da, namely, Da = 0.2, 0.5, 1, and 2.

Influence of Damköhler Number

In this section we consider a fixed value of the Reynolds number, Re = 10, and vary the value of the Damköhler number. Shown on Figs. 5 and 6 are the total mass of fuel and the maximum heat-release rate, respectively, versus time for four values of Da, namely, Da = 0.2, 0.5, 1, and 2.

The rate of change of the total mass of fuel with time can be interpreted as a global combustion rate. From Fig. 5 the effects of finite rate chemistry on this rate are obvious. Each of the individual curves in Fig. 6 exhibits the three stages I, II, and III introduced above. It is seen that, as it is to be expected, with decreasing values of the Damköhler number, i.e., with increasingly slower chemistry, stages I and II extend over *increasingly longer* periods of time. This in turn provides increasingly longer times for premixing of fuel and oxidizer and, as a consequence, once the stage of premixed flame propagation is complete, increasingly less fuel is available to be burnt in the diffusive stage III. Thus, with decreasing values of the Damköhler number stage III extends over *increasingly shorter* periods of time. In particular, as is

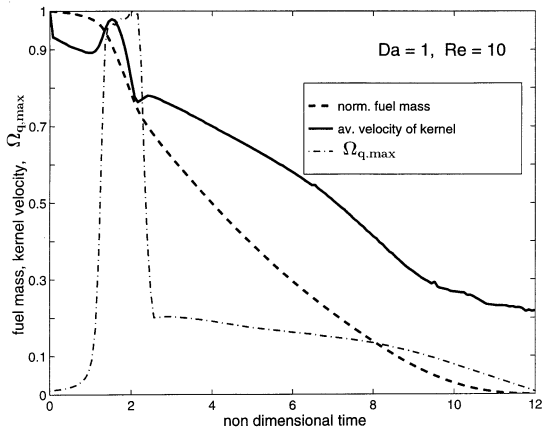

Fig. 4. Variation vs time of the average velocity U of the fuel kernel (solid line) and of the total mass of fuel $m_F(t)/m_F(0)$ (dashed line). Also the maximum heat release rate represented in Fig. 3 is included here as a dashed-dotted line.

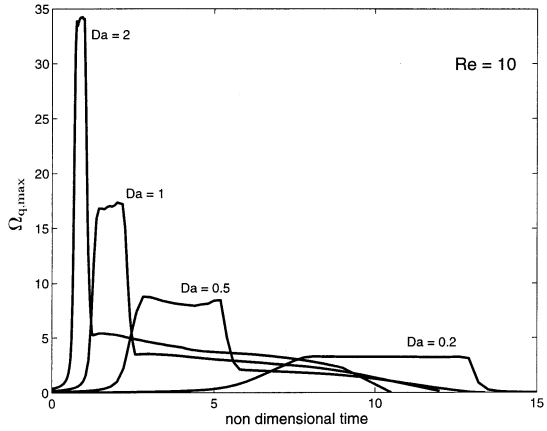

Fig. 6. Maximum heat-release rate versus time for Re = 10 and four values of Da, namely Da = 0.2, 0.5, 1, and 2.

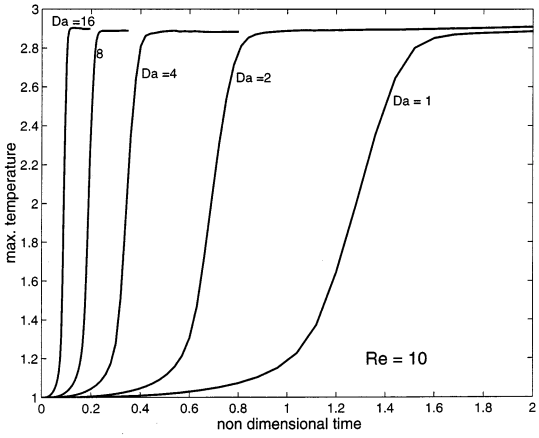

Fig. 7. Maximum flame temperature, θ_{max}, vs time for Da = 1, 2, 4, 8, and 16, respectively. Here Re = 10.

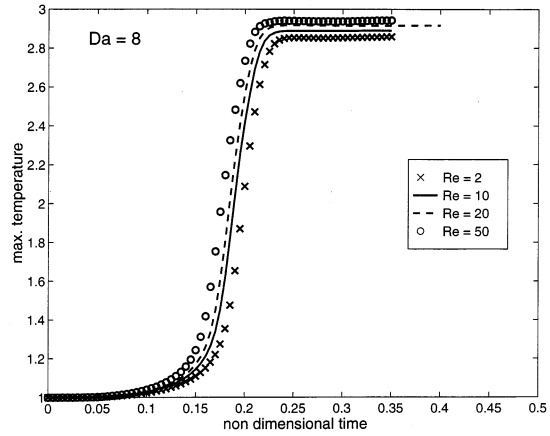

Fig. 8. Maximum flame temperature, θ_{max}, vs time for Re = 2, 10, 20, and 50, respectively. Here Da = 8.

illustrated in Fig. 6 for the case Da = 0.2, for sufficiently small values of the Damköhler number stage III *does not exist*, because the propagation velocity of the premixed flame originating at the back of the kernel and heading towards its nose is too small to overcome the velocity of the opposing flow. If we denote by S_L the burning velocity of the (triple) flame propagating during stage II circumferentially, normalized by the (initial) translational velocity of the kernel, the condition of non-existence of the diffusive stage can be expressed in terms of an order of magnitude estimate as $S_L \lesssim 1$. We shall come back to this point in detail when defining different regions in the Da-Re diagramme.

Influence of Reynolds Number and Damköhler Number on the Induction Time

In this section, we present some results that will be confirmed and explained by the analysis presented in the next Section.

In order to exhibit the dependence of the induction time, τ_{ind}, on the Damköhler number, plotted in Fig. 7 is the maximum flame temperature, θ_{max}, vs time for Da = 1, 2, 4, 8, and 16, respectively. From this figure it can be deduced that for sufficiently large values of the Damköhler number, τ_{ind} is inversely proportional to Da.

We now examine the influence of the Reynolds number, Re, on the induction time for a fixed large value of the Damköhler number, Da = 8, and determine τ_{ind} for four values of Re, namely, *Re* = 2, 10, 20, and 50. To this end we have plotted in Fig. 8 the maximum temperature vs time. The figure shows that the induction time is almost independent of Re for the (moderately) large value of Da under consideration.

Ignition-Combustion Regimes

In this section, we identify the ignition-combustion regimes that have appeared in the numerical simulations already described. To this end, we construct a Da-Re diagramme, which will also help to interpret and synthesize the results presented above. We start with some preliminary remarks.

Preliminaries

To prepare for the construction of the diagramme, it is helpful to make some remarks that introduce the characteristic scales appearing in the analysis.

(a) Consider first the planar configuration studied by Liñán and Crespo [19] consisting of two half spaces containing initially *fuel and oxidizer at rest*, respectively. In this configuration, a thermal runaway occurs after an induction time t^0_{ind} at which the mixing layer has grown to a typical thickness δ^0_{ind}. Note that here and below the superscript 0 is used to identify the characteristic scales of

this planar configuration. Assuming that the initial temperature of the oxidant, T_∞ say, is higher than that of the fuel and that the Lewis numbers are unity, $t^0_{\rm ind}$ and $\delta^0_{\rm ind}$ can be estimated as [19]

$$t^0_{\rm ind} = \frac{t_{\rm ch}(T_\infty)}{q \cdot \beta} \text{ and } \delta^0_{\rm ind} = \sqrt{D t^0_{\rm ind}}, \qquad (15)$$

respectively. Here q and β are the heat-release parameter and nondimensional activation energy, respectively, defined in Eqs. (8) and (11), and D is a characteristic diffusion coefficient; $t_{\rm ch}(T_\infty)$ is a chemical time evaluated at T_∞, with $t_{\rm ch}$ given as a function of temperature by

$$t_{\rm ch}^{-1} = B e^{-E/RT}. \qquad (16)$$

(b) In the previous sections we have shown that for sufficiently low values of the Damköhler number, ignition occurs in form of a thermal runaway at the back of the fuel kernel leading to a flame propagating circumferentially along the mixing layer towards the kernel nose. The propagating flame is expected to be a triple flame[5] because the mixture varies from rich to lean across the mixing layer. Let $S_{\rm L}$ be the velocity of propagation of this flame relative to the fresh mixture immediately ahead. A precise determination of $S_{\rm L}$ in the general case, which takes into account effects of nonuniformities in the flow field and in temperature and Lewis numbers across the mixing layer is difficult. For the present purposes, however, it is sufficient to neglect the effects of nonuniformities and to make the reasonable estimate that

$$S_{\rm L} = \sqrt{D/t_{\rm L}}, \qquad (17)$$

where $t_{\rm L}$ is the flame time of a stoichiometric planar deflagration with flame temperature $T_{\rm ad}$, given by Eq. (14). We will not need below an explicit form for $t_{\rm L}$, which is nevertheless available in the literature. For example, asymptotic analysis based on high activation energy (or an order-of-magnitude analysis as in [21] show that

$$t_{\rm L} \approx ({\rm Ze})^3 t_{\rm ch}(T_{\rm ad}), \qquad (18)$$

where $t_{\rm ch}(T_{\rm ad})$ is the chemical time evaluated at $T_{\rm ad}$, and Ze the Zeldovich number defined by ${\rm Ze} \equiv E(T_{\rm ad} - T_u)/RT^2_{\rm ad}$, T_u being the temperature in the fresh mixture. Because of the exponential Arrhenius factor in (16), $t_{\rm L}$ is typically smaller than $t^0_{\rm ind}$.

(c) Our last remark concerns the typical thickness of the mixing layer around the fuel kernel. This thickness will grow initially as $\sqrt{Dt}$ until it reaches an asymptotic value of order $\sqrt{Da_0/U_0}$.

[5] Although the tribrachial shape of the flame is absent for sufficiently low Da (see [20]).

Da-Re Diagramme

With the notations set above we now present a simple classification in the Da-Re diagramme. For sake of clarity, we remind the definitions adopted: ${\rm Da} = (a_0/U_0)/t_{\rm ch}(T_\infty)$ and ${\rm Re} = a_0U_0/D$, where a_0 denotes the initial radius of the kernel and U_0 its initial translational characteristic velocity relative to the surrounding oxidizing atmosphere.

We first plot two straight lines in this diagramme passing by the origin. The upper line is given by the equation ${\rm Da} = {\rm Re}/(q\beta)$; this equation is equivalent [on using (15)] to the condition that the Reynolds number based on $\delta^0_{\rm ind}$, ${\rm Re}_{\delta^0_{\rm ind}}$ is (of order) one, that is

$${\rm Re}_{\delta^0_{\rm ind}} \equiv \frac{\delta^0_{\rm ind} U_0}{D} \equiv \frac{\delta^0_{\rm ind}}{a_0}\,{\rm Re} = 1. \qquad (19)$$

The lower line corresponds to the condition $S_{\rm L} = U_0$, which can be written in non-dimensional form [taking into account (17)] as the linear relation

$${\rm Da} = \sigma\,{\rm Re}, \text{ with } \sigma = t_{\rm L}/t_{\rm ch}(T_\infty). \qquad (20)$$

The two straight lines given by Eqs. (19) and (20) subdivide the Da-Re plane into three distinct regions, which in Fig. 9 are labeled A, B, and C. The three regions can be characterized as follows.

In region A, the induction time $t_{\rm ind}$ is given by the induction time in the planar configuration, $t^0_{\rm ind}$. In other words the non-dimensional induction time $\tau_{\rm ind} \equiv t_{\rm ind}/(a_0/U_0)$ is given by the order of magnitude relation

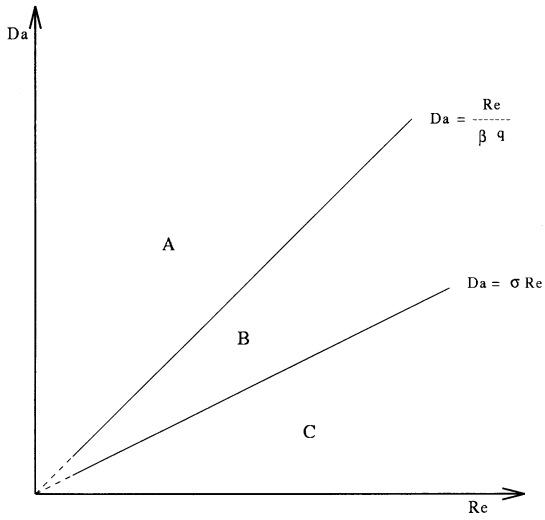

Fig. 9. Da/Re diagram for the ignition-combustion regimes. The upper straight line is given by the equation Da = Re/($q\beta$). The lower line corresponds to the condition $S_L = U$. In region A, the induction time t_{ind} is the same as in the planar configuration t^0_{ind} and ignition occurs in a spherical symmetric fashion. In region B ignition starts at the back and results in an established diffusion flame at front surface. In region C no diffusion flame at front. For illustration, Figs. 1 and 2 describe a case corresponding to region B, and Fig. 10 a case corresponding to region C. Note that the above diagram could be reproduced in terms of the unique parameter Da/Re.

$$\tau_{ind} \sim \frac{1}{q \cdot \beta \cdot \mathrm{Da}}. \tag{21}$$

Equation (21) shows that τ_{ind} is inversely proportional to the Damköhler number and independent of the Reynolds number, a finding that explains the numerical results relative to induction above.

We now justify our claim that in this region $t_{ind} = t^0_{ind}$. To this end it is sufficient to note that, at any location of the mixing layer the situation is locally the same as in the planar geometry and, therefore, we have $t_{ind} = t^0_{ind}$, provided that two conditions are satisfied:

- the streamwise convection along the mixing layer is negligible (compared to transverse diffusion)
- the curvature of the mixing layer can be discarded.

The relative importance of the streamwise convection, compared to transverse diffusion, is suitably expressed (during t^0_{ind}) in terms of the Reynolds number

$$\mathrm{Re}_{\delta^0_{ind}} = \frac{\delta^0_{ind} U_0}{D} = \mathrm{Re}\,\frac{\delta^0_{ind}}{a}. \tag{22}$$

In order for the effects of streamwise convection to be negligible, obviously $\mathrm{Re}_{\delta^0_{ind}} < 1$ is required. From (22) it is seen that if $\mathrm{Re}_{\delta^0_{ind}} < 1$, then, provided that Re is at least of order unity, $\delta^0_{ind}/a \ll 1$ is a consequence. The latter inequality justify that curvature can be neglected.

In region B, the effects of the convective flow relative to the kernel will be felt during ignition. Consequently, ignition will not occur (nearly) uniformly and simultaneously along the periphery of the kernel, but, as the numerical results indicate, will take place at the kernel's back, followed by flame propagation towards the nose with a relative velocity of the order of S_L. As the maximum flow velocity (relative to the fuel kernel), which is reached at the equator of the kernel, is of order U_0, the flame will not be able to reach the nose unless $S_L > U_0$. If the latter condition is not satisfied, the stage of diffusive burning is not established at the front.

In region C two scenarios are possible. The first follows immediately from above: For $S_L < U_0$, a flame may stabilize at the back of the kernel in which (essentially premixed) combustion takes place until all fuel is exhausted. A flame under such conditions is the flame discussed above in the context of Fig. 6, viz., the flame for Da = 0.2. A sequence of temperature and heat release surface plots for this flame is shown in Fig. 10. The second possible scenario takes place if the chemistry is sufficiently slow for complete premixing to take place prior to ignition. As a consequence, once ignition has occured in the latter case, combustion will take place exclusively in the premixed mode.

Remarks

In the discussion above, the Reynolds and Damköhler numbers appearing in the diagramme have been treated as constant characteristic parameters, based on the initial values of the physical parameters. Nevertheless, for some purposes it can be useful to consider them as instantaneous parameters which vary on a time scale much larger than a typical chemical time, say t_L. Such slow variations associated with the decrease of the translational velocity U of the

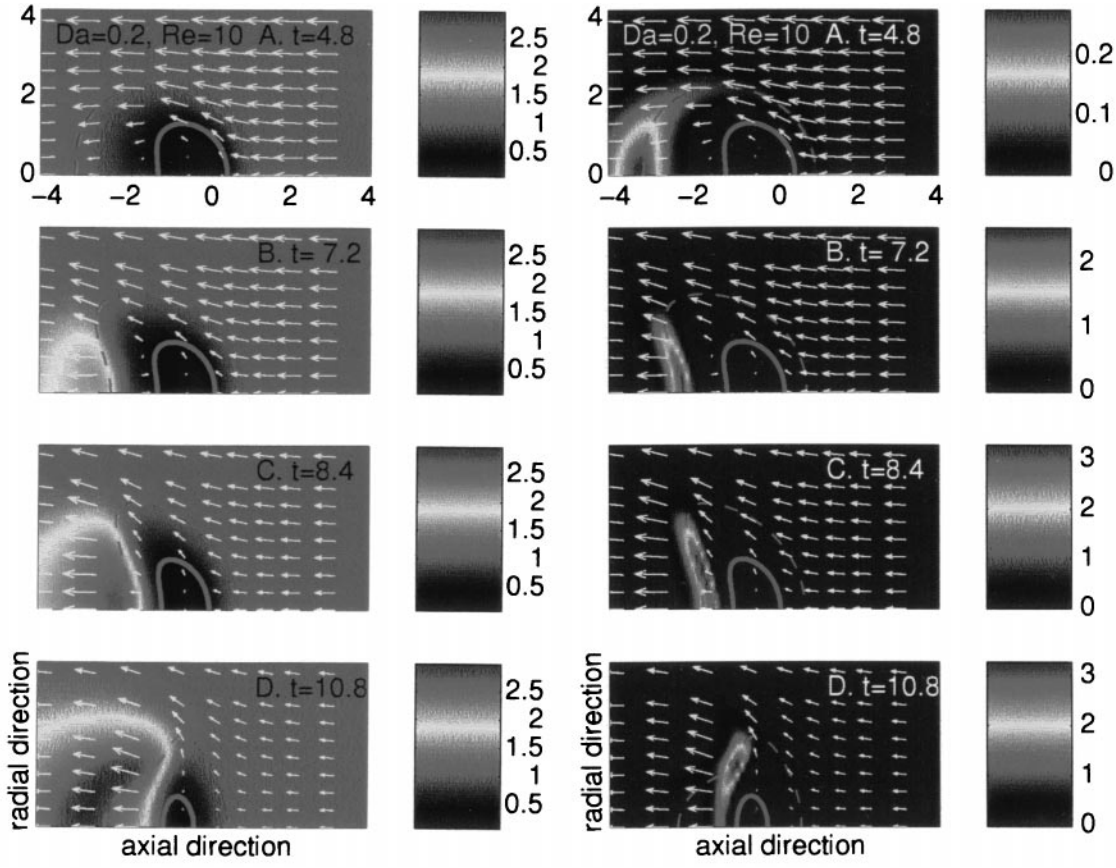

Fig. 10. A sequence of temperature (respectively, heat release rate) surface plots corresponding to Da = 0.2 and Re = 10. The pictures pertain, respectively, to $t = 4.8$, 7.2, 8.4, and 10.8.

fuel kernel and its radius a are, for example, expected for sufficiently dense fuel kernels (i.e., for $\epsilon \ll 1$). Consequently, as time evolves, a point on the diagramme describing the state of the fuel kernel can move from one region to another. For example, consider a fuel kernel moving with a sufficiently high velocity so that its representative point P in the diagramme lies in region C. A possible scenario would consist in a runaway at the back followed by an established burning with the flame remaining at the back (P in region C, but progressing towards region B) until the velocity of the kernel U decreases below S_L (P has reached region B); the flame then reaches the nose establishing a diffusion flame at the front surface. It is interesting to note that such transient behaviour can also be found in the numerical simulation of the combustion of a moving drop by Dwyer and Sanders [11].

Our last remark concerns the stability of the (quasi-steady) position of the triple flame established at the back of the kernel, near the equator.[6] It is clear that this position is stable because locally the velocity of the opposing flow relative to the kernel, say $\boldsymbol{V}$, increases in the direction of propagation (i.e., around the kernel from back to equator); under such conditions it is indeed clear that any infinitesimal displacement of the flame is opposed by the flow. In other words, denoting by $\boldsymbol{n}$ a unit vector along the mixing layer pointing to the fresh mixture in the direction of propagation, the position occupied by the flame is stable, because at this position the two conditions

$$S_L = -\boldsymbol{V}\cdot\boldsymbol{n} \text{ and } \boldsymbol{n}\cdot\nabla(-\boldsymbol{V}\cdot\boldsymbol{n}) > 0 \qquad (23)$$

[6] This remark concerns region C of the Da-Re diagramme.

are met. Evidently no such stable steady triple flame can be realized at the front surface because the second condition in (23) is never satisfied. For example, consider the case of a moving kernel (or droplet) with an established diffusion flame at front. If the relative velocity between the kernel and the ambiance is increased then we can expect extinction to occur at the front stagnation point (where the strain is maximum), leaving a hole on the flame around the stagnation point. The border of the hole is typically a triple flame. Because this flame is unstable, the hole will grow until it embraces the equator. Stable combustion goes on at the back, unless the relative velocity is again decreased.

CONCLUSIONS

In this paper the ignition and combustion of an initially spherical fuel kernel impulsively moved in a hot oxidizing gas are investigated. Attention is focused on finite rate effects, the chemistry being modeled by a single irreversible Arrhenius reaction. Unless the chemistry is too fast or too slow, three stages are identified in the burning process. Stage I corresponds to an induction period during which a mixing layer is formed and ends with a thermal runaway at the back of the kernel. Stage II involves the propagation of a (triple-) flame around the kernel until the nose is reached. Stage III corresponds to an established diffusive burning. At high values of the Damköhler number, Da, ignition occurs in a spherical fashion and the induction time is independent of the Reynolds number, Re, and inversely proportional to Da. For low values of Da, stage III is practically absent. The numerical results are complemented by an order-of-magnitude analysis allowing classification of the observed phenomena in the Da-Re plane. Finally, it is worth noting that we have limited ourselves in this study to moderate values of the Reynolds number (say a few tens) and did not discuss fluid mechanical aspects of the problem (such as kernel deformation, influence of the Reynolds number on the combustion rate, effects of heat release and so on). Those aspects have been studied independently in the framework of a flame sheet model [16].

The present study was supported by the Commission of the European Communities within the frame of the Programme "Gravity Dependent Phenomena in Combustion" and postdoctoral grant number ERBFM-BICT961503. The author is grateful to Prof. Bernd Rogg for his active help and useful suggestions concerning this work and to Prof. Amable Liñán for fruitful discussions.

REFERENCES

1. Faeth, G. M., Dominicis, D. P., Tulpinski, J. F., and Olson, D. R. (1969). *12th Symposium Internal Combustion*, The Combustion Institute, Pittsburgh, p. 9.
2. Sato, J., Tsue, M., Niwa, M., and Kono, M., *Combust. Flame*, 82:142–150 (1990).
3. Spalding, D. B., *ARS J*. 29:828 (1958).
4. Sanchez-Tarifa, C., Crespo, A., and Fraga., E., *Astro. Acta*, 17:685 (1972).
5. Daou, J., Haldenwang, P., and Nicoli, C., *Combust. Flame*, 101:153 (1995).
6. Haldenwang, P., Nicoli, C., and Daou, J., *Int. J. Heat Mass Trans*., 39:3453–3464 (1996).
7. Shuen, J. S., Yang, V., and Hsiao, C. C., *Combust. Flame*, 89:299–319 (1992).
8. Umemura, A., and Shimada, Y. (1996). *26th Symposium Internal Combustion*, The Combustion Institute, p. 1621.
9. Prakash, S., and Sirigiano, W. A., *Int. J. Heat Mass Trans*., 23:253–268 (1980).
10. Fernandez-Pello, A. C., *Comb. Sci. Tech*., 28:305–313 (1982).
11. Dwyer, H. A., and Sanders, B. R., (1988). *22nd Symposium Internal Combustion*, 1923–1929.
12. Dwyer, H. A., and Sanders, B. R., *Comb. Sci. Tech*., 58:253 (1988).
13. Deng, Z. T., Litchford, R., and Jeng, S. M., *AIAA* 92–3122 (1992).
14. Lee, H. S., Fernandez-Pello, A. C., Corcos, G. M., and Oppenheim, A. K., *Combust. Flame*, 81:50–58 (1990).
15. Daou, J., and Haldenwang, P., *Eur. J. Mechanics, B/Fluids* 16:141–161 (1997).
16. Daou, J., and Rogg, B., *Combust. Flame* 115:145–157 (1998).
17. Umemura, A., and Jia, W., In *Modeling in Combustion Science*, (J. D. Buckmaster and T. Takeno, Eds.), Springer-Verlag, Berlin, 1995, p. 237.
18. Ruge, J., and Stüben, K., In *Proceedings of the Multigrid Conference*, Bristol, Sept. 1983.
19. Liñán, A., and Crespo, A., *Comb. Sci. Tech*., 14:95–117 (1976).
20. Kioni, P. N., Rogg, B., Bray, C., and Liñán, A., *Combust. Flame*, 95:276–290 (1993).
21. Liñán, A., and Williams, F. A., *Fundamental Aspects of Combustion*, Oxford Univ. Press, New York, 1993.

Received 1 September 1997; revised 5 December 1997; accepted 16 December 1997